Spring 5-15-2023

Single-Molecule Super-Resolution Imaging of Geobacter sulfurreducens under Anaerobic Conditions

Ziyi Hu

WASHINGTON UNIVERSITY IN ST. LOUIS

McKelvey School of Engineering
Department of Biomedical Engineering

Thesis Examination Committee:
Matthew D. Lew, Chair
Daniel Bond
Michael Vahey

Single-Molecule Super-Resolution Imaging of *Geobacter sulfurreducens* under Anaerobic Conditions

by
Ziyi Hu

A thesis presented to
the McKelvey School of Engineering
of Washington University in
partial fulfillment of the
requirements for the degree
of Master of Science

May 2023
St. Louis, Missouri

Table of Contents

List of Figures

List of Tables

Acknowledgments

I would like to express my sincere gratitude to Dr. Matthew D. Lew, my thesis advisor, for his unwavering guidance and thoughtfulness throughout the past two years of my research. Without his support, this thesis would not have been possible. I would also like to extend my thanks to Sol Choi, our collaborator, for her invaluable assistance in teaching me how to handle the *Geobacter* and providing us with the cells needed for our experiments. Their contributions have been indispensable to the success of this project. My gratitude also goes to Dr. Michael Vahey and Dr. Daniel Bond, my committee members, for their insightful comments and helpful feedback, which greatly improved the quality of my work.

I would also like to thank Lew lab alumni Dr. Jin Lu and Dr. Tianben Ding for teaching me the necessary experimental skills to operate the microscope. Additionally, I would like to thank the current members of the Lew lab for their valuable insights during our group meetings. My heartfelt appreciation also goes to my friends Sili Xu, Yunyun Yang, Liwen Lin, Chiaying Kuo, and my cat Elmo for their emotional support, which sustained me throughout these two years.

Lastly, I want to express my profound gratitude to my parents for their unwavering love and support along the way. Their encouragement has been a source of strength and inspiration for me.

Ziyi Hu

Washington University in St. Louis

May 2023

Dedicated to my parents and friends who have always supported me and pushed me to achieve the best.

ABSTRACT OF THE THESIS

Single-Molecule Super-Resolution Imaging of *Geobacter sulfurreducens* under Anaerobic Conditions

by

Ziyi Hu

Master of Science in Biomedical Engineering

Washington University in St. Louis, 2023

Professor Matthew D. Lew, Chair

Geobacter sulfurreducens are anaerobic bacteria capable of making electrical contacts with other organisms and extracellular electron acceptors. The challenge of imaging live *Geobacter* bacteria is maintaining anaerobic conditions during the imaging process. In this thesis, we augment a single-molecule localization microscope (SMLM) with a home-built anaerobic imaging chamber and use constant argon bubbling to maintain oxygen-free imaging conditions. To validate the imaging protocol, we use the transient binding of Nile red to resolve the spherical morphology of lipid-coated glass spheres with nanoscale resolution. However, when imaging *Geobacter*, the distribution of Nile red localizations is non-uniform, both between different cells on a single coverslip as well as along individual cell membranes. We hypothesize that *Geobacter*'s ability to transfer electrons extracellularly can reduce single Nile red molecules, thereby transforming them into a dark, non-fluorescent state. We quantitatively compare Nile red activity on wild-type *Geobacter* to a mutant whose major outer membrane porin-cytochrome complexes are deleted. We demonstrate that SMLM has great potential for quantifying oxidation-reduction activity at the single-molecule level in living bacteria.

Chapter 1: Introduction

Single-molecule localization microscopy is a powerful tool for examining biological samples with nanoscale resolution, revealing fine structures of cells and proteins. *Geobacter sulfurreducens*, a well-studied member of the *Geobacteraceae* family, is an anaerobic bacterium capable of establishing electrical contacts with other organisms and extracellular electron acceptors.

This thesis focuses on single-molecule imaging of *Geobacter sulfurreducens* under anaerobic conditions. The first chapter provides a comprehensive background on the topic. Section 1.1 introduces *Geobacter sulfurreducens*, while section 1.2 discusses single-molecule localization imaging. Section 1.3 highlights the challenges of performing single-molecule imaging under anaerobic conditions.

1.1 *Geobacter sulfurreducens*

Geobacter sulfurreducens was first discovered in Norman, Oklahoma, by F. Caccavo Jr. et al [1]. It is a rod-shaped bacterium belonging to the *Geobacteraceae* family and is commonly found in sedimentary environments such as riverbeds and geological compounds where there is a lack of oxygen.

These bacteria are capable of using nanowires to grow as electroactive biofilms on electrodes, converting electrons into electricity and conducting electricity as a result. *Geobacter sulfurreducens* is of interest for extracellular electron transfer studies.

For our study, we used both the wild-type *Geobacter sulfurreducens* and a mutant lacking outer membrane cytochromes, referred as Δ5. The mutant strain had five conduit gene clusters deleted: *extABCD*, *extEFG*, *extHIJKL*, *omcB*-based and *omcC*-based clusters [2]. All the *Geobacter*

samples used in this study were prepared by our collaborator, Sol Choi, from the Bond lab in the University of Minnesota-Twin Cities.

1.2 Single-molecule localization imaging

Single-molecule localization microscopy (SMLM) [3–6] is a powerful imaging technique that significantly improves spatial resolution beyond the diffraction limit, enabling imaging of biological structures at nanometer scale. Conventional fluorescence microscopes cannot precisely locate individual molecules because all fluorescence molecules emit simultaneously, resulting in a blurry image. However, SMLM overcomes this issue by having only a limited number of blinking events per frame. This technique can accurately determine the emitter's position in each frame, and by combining multiple frames, a nanoscale resolution image can be reconstructed.

In our study, we utilized the point accumulation in nanoscale topography (PAINT) [7] with Nile red molecules. Nile red is non-fluorescent in aqueous solution, but it becomes fluorescent in hydrophobic environment such as cell walls [8].

1.3 Challenges for single-molecule imaging under anaerobic conditions

In our lab, we typically utilize an 8-well chambered cover glass or the glass coverslip with a silicone chamber for standard single-molecule imaging (Figure 1.1 (a) and (b)). However, due to the confined space within these chambers, it is not possible to incorporate gas in and out lines to maintain an anaerobic environment. Additionally, the typical *Geobacter* electrochemical experiment chamber (Figure 1.1 (c), developed by the Bond lab, University of Minnesota-Twin

Cities), is too large to be accommodated by our microscope, and the glass material are not suitable for the single-molecule localization microscopy (SMLM) imaging. These challenges motivated us to design a new anaerobic imaging chamber, as described in Chap 2 Section 2.3.

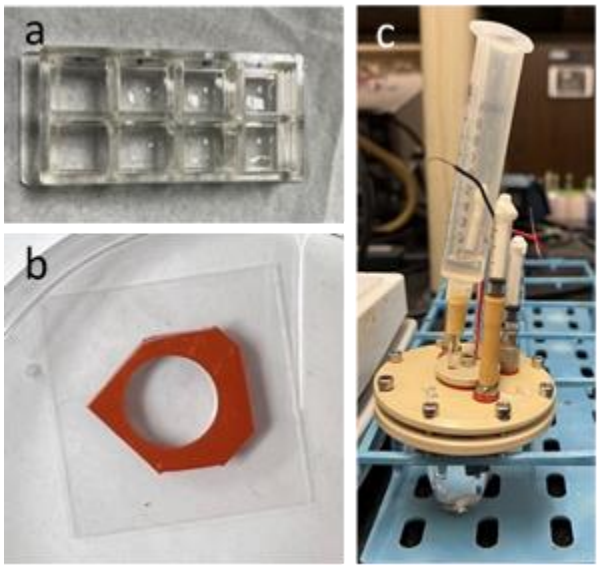

Figure1. 1 Imaging chamber in Lew lab and *Geobacter* electrochemical experiment chamber from Bond lab. (a) 8-well chambered cover glass (57.00 mm X 25.00 mm X 10.8 mm) (b) glass coverslip with a silicone chamber (coverslip: 22 mm X 22 mm, volume: 200 uL) (c) *Geobacter* electrochemical experiment chamber

Chapter 2: Methods

This chapter introduces the experimental methods, including the supported lipid bilayer (SLB) coated spherical silica beads preparation, *Geobacter* cell culture, imaging chamber design, imaging procedure and the super-resolution imaging analysis.

2.1 Preparing supported lipid bilayers (SLBs) on silica spheres

To prepare spherical glass beads coated with a supported lipid bilayer, we began by creating large unilamellar vesicles (LUVs). We added 19.09 μL of 25 mg/mL DPPC in chloroform (1, 2-dipalmitoyl-sn-glycero-3-phosphocholine, Avanti Polar Lipids, 850355P-25mg, Lot# 850355200MGA326) to the empty test tube, and then evaporated it under vacuum overnight (for 12 hours). Next, 0.65 mL Tris buffer (100 mM NaCl, 3 mM CaCl2, 10 mM Tris, pH 7.4) was added to reach a final lipid concentration of 1 mM. We then formed a lipid suspension by vortexing the mixture above 41 ℃ for 40 minutes, followed by extrusion (25 passages, using an Avanti Mini-Extruder, Avanti Polar Lipids).

Before coating the LUVs to the 1.97 μm silica beads (SS04002, Bangs Laboratories Inc), we first clean them by replacing the original bead solvent with Tris-Ca^{2+} buffer (100 mM NaCl, 3 mM CaCl2, 10 mM Tris, pH 7.4). We then mixed the cleaned silica beads solution with the LUVs and incubated the mixture in the water bath at 65 ℃ for 30 min, vortexing the tube every 5 minutes to ensure thoroughly mixing. Next, we transferred 65°C water from the water bath to a separate container and placed the tube containing the mixture in the new bath. After allowing the mixture to cool to room temperature over the course of an hour, we centrifuged it for 5 minutes at 600 rpm, repeating this step six times. After each centrifuge, we removed the top 2/3 of the supernatant and

replaced it with Ca^{2+} free Tris buffer (100 mM NaCl, 10 mM Tris, pH 7.4), thoroughly vortexing the tube before proceeding to imaging.

2.2 *Geobacter* cell culture

Figure 2. 1 Anaerobic pressure bottle and tube. (a) The anaerobic pressure bottle, which consists of three parts, the glass bottle, the blue rubber plug and the aluminum ring. The aluminum ring was clamped to ensure the plug stayed on the bottle during autoclave. (b) The anaerobic pressure tube.

Geobacter sulfurreducens strains were cultured in an anaerobic growth medium containing 20 mM acetate as the electron donor and 40 mM fumarate as the electron acceptor at 30°C. The growth

medium, as described in Sol's paper [9], consisted 0.38 g/L KCl, 0.2 g/L NH_4Cl, 0.069 g/L $NaH_2PO_4 \cdot H_2O$, 0.04 g/L $CaCl_2$, 0.2 g/L $MgSO_4 \cdot 7H_2O$, 10 mL/L of a trace mineral mix, adjusted to pH to 6.8 and buffered with 2 g/L $NaHCO_3$. The trace mineral mix comprised 1.5 g/L nitrilotriacetic acid (NTA), 0.1 g/L $MnCl_2 \cdot 4H_2O$, 0.5 g/L $Fe_2SO_4 \cdot 7H_2O$, 0.17 g/L $CoCl_2 \cdot 6H_2O$, 0.10 g/L $ZnCl_2$, 0.03 g/L $CuSO_4 \cdot 5H_2O$, 0.005 g/L $AlK(SO_4)_2 \cdot 12H_2O$, 0.005 g/L H_3BO_3, 0.09 g/L Na_2MoO_4, 0.05 g/L $NiCl_2$, 0.02 g/L $NaWO_4 \cdot 2H_2O$, 0.10 g/L Na_2SeO_4.

To ensure anaerobic conditions, the growth media were dispensed into anaerobic pressure tubes with rubber stoppers and bubbled with an 80% N_2 and 20% CO_2 gas mixture for 15 minutes.

To ensure anaerobic conditions, the growth media were dispensed into anaerobic pressure tubes with rubber stoppers (Figure 2.1, Chemglass Life Sciences, NJ) and bubbled with 80% N_2 and 20% CO_2 gas mixture for 15 minutes. Before each imaging experiment, the optical density of *Geobacter* was checked using a 594 nm laser (Cobolt Mambo™) and power meter (Newport, 1918-R).

2.3 Imaging chamber design

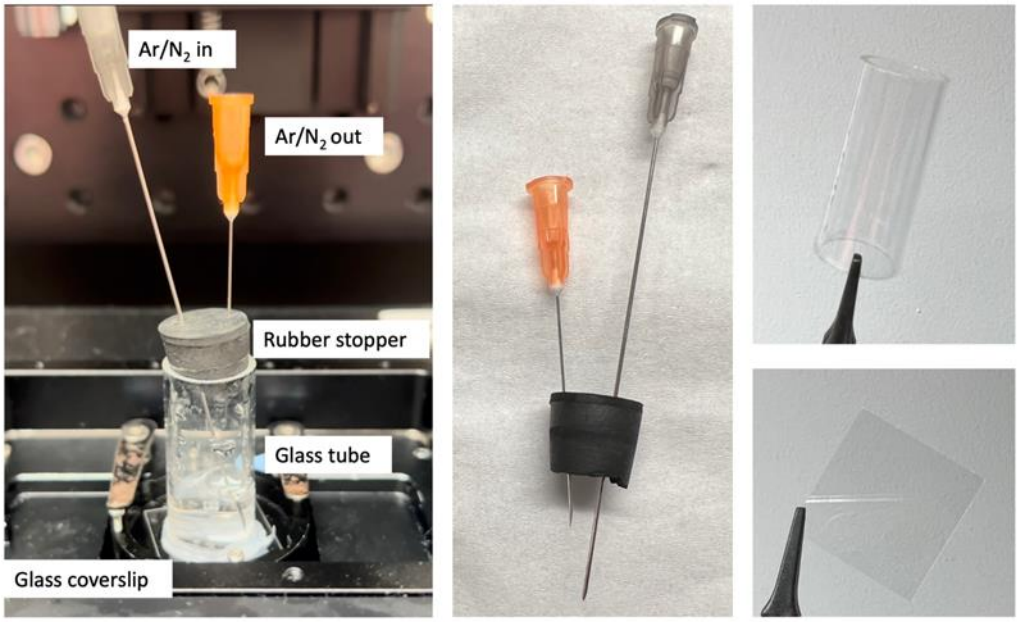

Figure 2. 2 Anaerobic imaging chamber. (a) The anaerobic imaging chamber on the microscope. comprising of a (b) rubber stopper, two needles serving as the gas in and out line (Exel Hypodermic Needles 25G x 1.5 in, Air-Tite™ Premium Hypodermic Needles for Lab/Vet Use 22G x 3 in), a (c) glass tube costumed made by the WashU glass shop (outer diameter 15mm, height 30 mm), and a (d) a high-precision coverslip (Marienfeld, No. 1.5H, thickness 170 µm±5 µm, 22×22 mm).

Figure 2.2 shows the complete imaging chamber and its various components, comprising of a glass tube, a high-precision coverslip, and two needles serving as gas in and out lines. To assemble the chamber, we applied silicone gel (White Lightning, Silicone Ultra-Kitchen and Bath, W21101005) to the rim of the glass tube and gently pressed it onto the coverslip. We allowed the assembly to air dry for at least four hours before use. During imaging, the needle of the gas in line should be positioned under the surface of the solution.

2.4 Imaging procedure

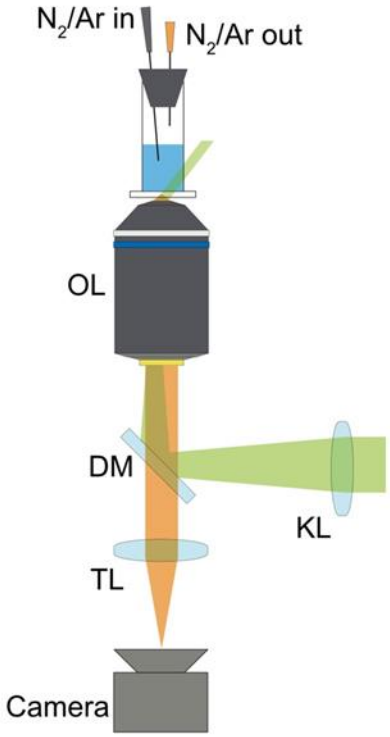

Figure 2. 3 Schematics of the fluorescence microscope. Schematics of the fluorescence microscope. KL: Kohler lens. TL: tube lens. DM: dichroic mirror. OL: objective lens.

The imaging chamber was cleaned by using a UV Ozone Cleaner (Novascan Technologies) for 15 minutes. Next, we took 1 mL of *Geobacter sulfurreducens* solutions from the growth media tube with an optical density ranging from 0.3-0.5 and added it to a 1.5 mL microcentrifuge tube. After centrifuging the solution for 1 minute at 6,000 g, we discarded the supernatant and added 1.5 mL of *Geobacter* imaging buffer (50 mM NaH_2PO_4, 50 mM NaCl, 0.8 mM $MgSO_4 \cdot 7H2O$, 0.3 mM $CaCl_2 \cdot 2H_2O$, 30 mM HEPES, pH 6.8). We redispersed the *Geobacter* in the imaging buffer by vortexing and incubated it for 1 hour with constant Argon bubbling. We then replaced the buffer with a fresh 1.5 mL *Geobacter* imaging buffer to remove any floating cells. For Nile red imaging,

we added 6 µL of 10 µM Nile Red (Fisher Scientific, AC415711000) in *Geobacter* imaging buffer to the imaging chamber, reaching a final concentration of 40 nM.

2.5 Single-molecule image processing

To obtain a super-resolution reconstruction of NR blinking events, we processed the raw data with ThunderSTORM [10] plugin on ImageJ [11]. The software consists of three main parts: image filtering and feature enhancement, finding approximate positions of molecules, and sub-pixel localization of the molecule.

For the raw data collected in this thesis, we used the B-Spline wavelet in ThunderSTORM for denoising and feature enhancement. To obtain approximate locations of each blinking event, we used the detection of local intensity maxima as described in the ThunderSTORM paper. An integrated Gaussian function was used to fit the single-molecule intensity distributions, accounting for the pixelation effects and the presence of noise. Maximum-likelihood estimation was used to fit the integrated Gaussian function, as previously described. Prior to import the data to ThunderSTORM, we corrected the camera offset by subtracting it from the raw fluorescence images using the subtraction function in ImageJ. We then used ThunderSTORM to process the offset-subtracted raw data.

A list of single-molecule position (x, y) estimates along with the intensity information and the PSF width, was generated by ThunderSTORM. To ensure the accuracy of our results, we applied the ThunderSTORM built-in intensity filter to identify single molecules with an intensity over 100, which helped reject false localizations caused by background fluorescence and low signal-to-noise ratio. The resulting list of single-molecule positions, along with their intensity information, was

exported as a CSV file and loaded into MATLAB (Mathworks, R2021b) for further post-processing.

2.5.1 Quantifying fluorescence burst duration

We combine single molecules localized in a frame with those in the next few frames by selecting the closest neighbors with a spatial distance within three times of the localization precision. The localization precision σ_{LS} of a least squares SMLM algorithm is given by

$$\sigma_{LS} = \sqrt{\frac{s^2+a^2/12}{N}\left(\frac{16}{9}+\frac{8\pi\left(s^2+\frac{a^2}{12}\right)b}{Na^2}\right)} \qquad (2.1)$$

where N is the detected photon, s is the standard deviation of the 2D Gaussian function that describes the microscope's PSF, a is the camera pixel size, and b is the photon background. We quantified the duration of each burst, or the time the SM stayed "on", by counting the number of frames in which localizations were grouped together, measured in units of exposure time.

2.5.2 Selecting regions of interest (ROIs) corresponding to single *Geobacter* cells

Geobacter were visualized by binning all single molecules from one image stack (20k frames) in post-processing. To extract single-molecule activity solely from *Geobacter*, we selected single-cell regions of interest (ROIs) for *Geobacter*. The contour was hand-drawn using the *drawfreehand* function in MATLAB (Mathworks, 2021b). Subsequently, the contour was dilated using the *imfill* function in MATLAB. To further refine our analysis, we applied the filled mask to the original SMLM image, which enabled us to count only the localizations within the mask for further post-processing.

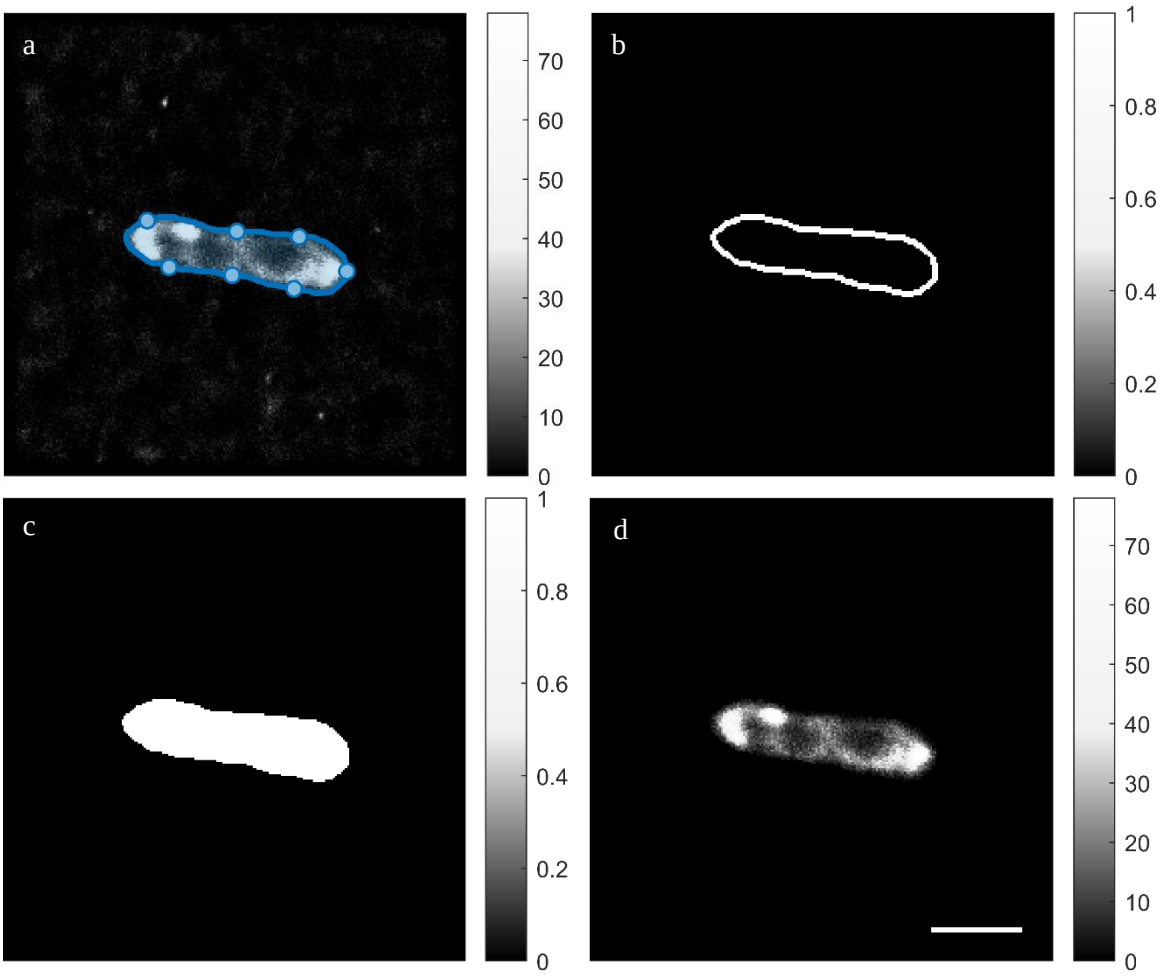

Figure 2. 4 Region of interest selection of *Geobacter* single cell. (a) The reconstructed SMLM image with all the localizations, blue line is the hand draw ROI. (b) The binary mask image of the ROI (c) Dilated image from the binary mask (d) Single *Geobacter* SMLM reconstructed image with only the localizations within the mask. Color bar: number of localizations per bin (20×20 nm^2). Scale bar: 1 μm.

Chapter 3: Results

This chapter shows our capability to resolve the structure of lipid-coated beads with single-molecule sensitivity. We are able to provide evidence that *Geobacter* remains viable in our imaging chamber during the imaging process. Single-Molecule Localization Microscopy (SMLM) shows that Nile red localizes non-uniformly on and within *Geobacter*. We also conduct a quantitative analysis to compare Nile red activity between wild-type *Geobacter* and the outer membrane cytochrome-deleted mutant.

3.1 SMLM imaging of supported lipid bilayer (SLB)-coated glass spheres

To demonstrate the efficacy of Single-Molecule Localization Microscopy (SMLM) under anaerobic conditions, we used 2µm SLB-coated glass beads as imaging targets to characterize the transient binding of Nile red. After preparing SLB-coated glass spheres (Chapter 2.1), we extracted 10 µL of the solution for imaging. First, we placed the SLB-coated glass sphere solution into the anaerobic imaging chamber (as described in Chapter 2.3) and added 1.5 mL Ca2+-free Tris buffer (the same buffer used to store the SLB-coated glass sphere) as the imaging buffer. The Ca2+-free Tris buffer was pipetted into the imaging chamber to reach a final Nile red concentration of 40 nM. For the experiment without oxygen, argon was constantly flowing into the chamber during the imaging process. For the experiment in the presence of oxygen, we imaged the same sample after removing the plug on the imaging chamber and waiting for 20 minutes to let the imaging buffer mix with the air. We recoded a total of 20k frames with 20 ms camera exposure for each reconstruction. Using ThunderSTORM, we reconstructed SMLM images with 20 nm × 20 nm bin

size, successfully visualizing the circular shape of the SLB-coated glass sphere. During the experiment, we imaged a total of 14 field of views under anaerobic conditions (Figure 3.1) and 9 field of views under aerobic conditions (Figure 3.2).

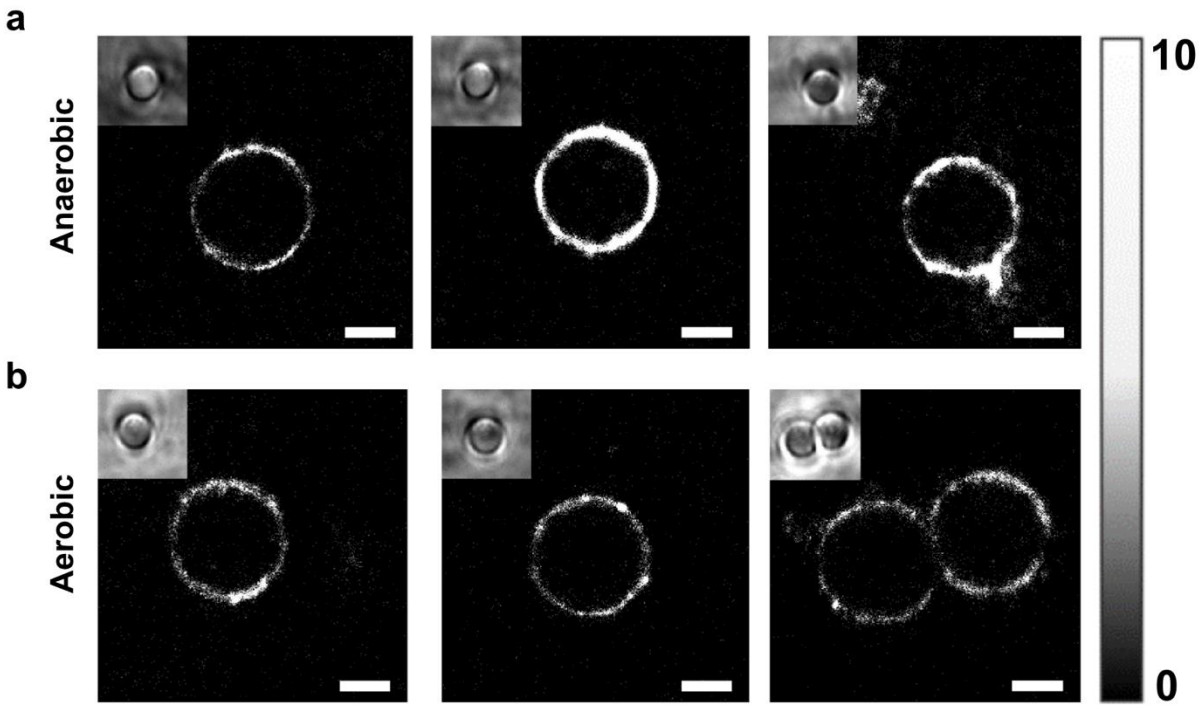

Figure 3. 1 SMLM images SLB-coated sphere under anaerobic and aerobic conditions. Upper left image is a bright field image of the same bead. Scale bar: 1 μm. Color bar: number of localizations per bin.

In addition to reconstructing the SMLM images of the SLB-coated glass sphere, we also calculated the burst duration (Chapter 2.5) with both oxygen present and absent. We found that the median percentage of burst duration over 60 ms for the oxygen-absent cases was 1.4% larger than the ones exposed to air. The median mean burst duration of Nile red under anaerobic conditions was 1.6 ms higher than that with oxygen present (Figure 3.4 (c) and (d)).

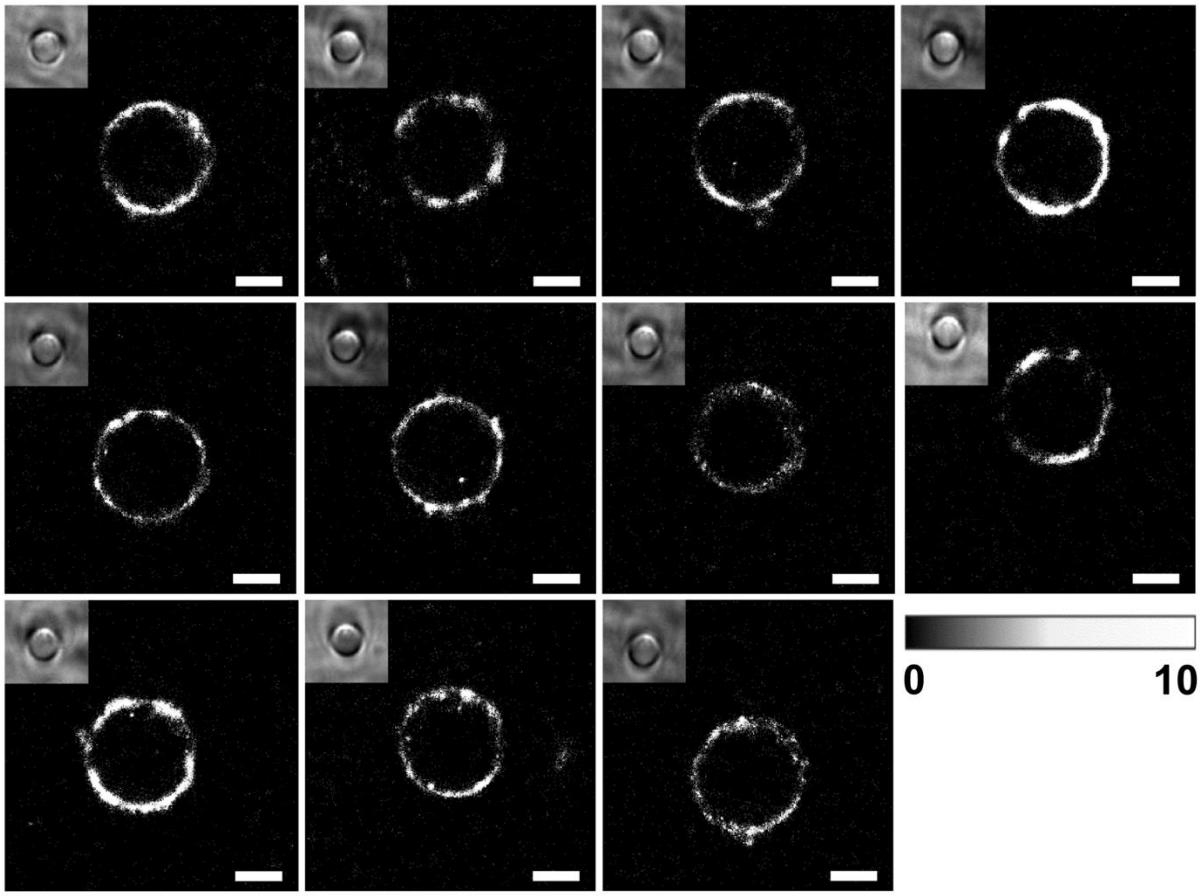

Figure 3. 2 SMLM image gallery of SLB-coated spheres under anaerobic conditions. Upper left image is the bright field image of the same bead. Scale bar: 1 μm. Color bar: number of localizations per bin.

Generally, anaerobic conditions increase fluorophore longevity [12] by slowing dye photobleaching [13], which could explain the slight increase of the mean burst time for the no-oxygen cases. However, if the dominant turn-off mechanism for the Nile red dye is unbinding rather than photobleaching, then we expect oxygen-related turn-off to be insignificant in our

experiments. Thus, the minimal differences observed between the oxygen and no-oxygen cases suggests that the primary Nile red blinking mechanism is transient binding [14].

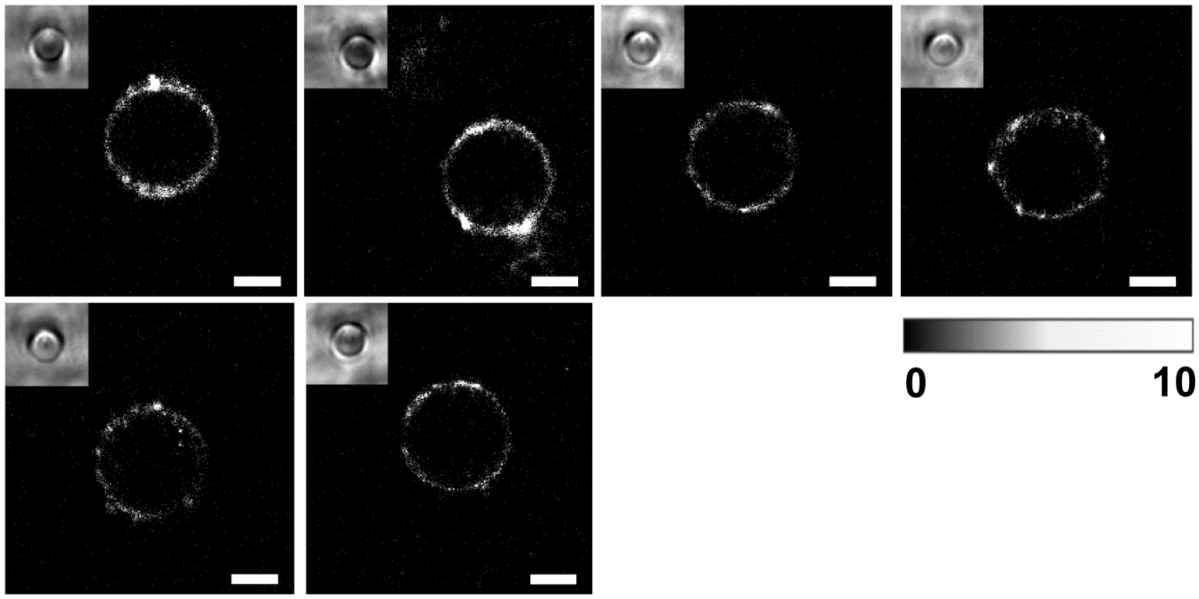

Figure 3. 3 SMLM image gallery of SLB-coated spheres under aerobic conditions. Upper left image is the bright field image of the same bead. Scale bar: 1 μm. Color bar: number of localizations per bin.

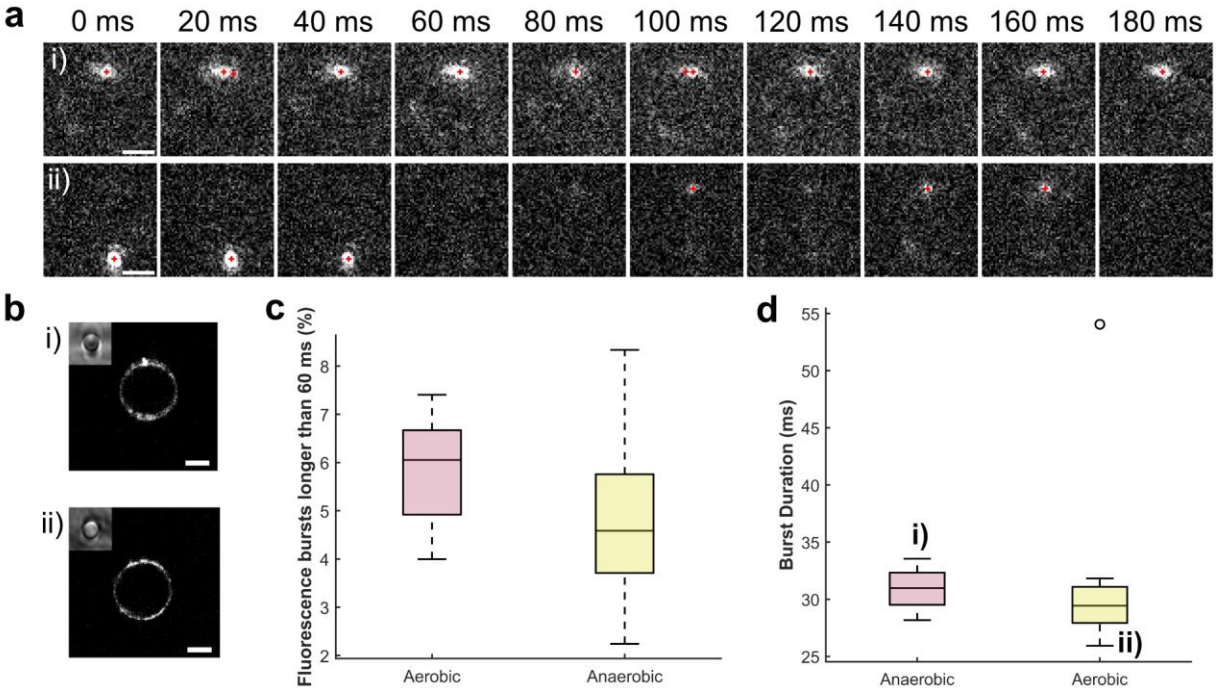

Figure 3. 4 Quantifying Nile red fluorescence bursts on SLB-coated glass spheres. (a) Raw images of 10 consecutive frames with the red cross as the PSF center. This molecule has the shortest mean burst duration for in the oxygen-absent experiment. (b) i) SMLM reconstructed image of the sphere in (a) i). (c) Fraction of burst durations over 60 ms under anaerobic and aerobic conditions. (d) Mean burst duration distribution of Nile red under anaerobic and aerobic conditions. Scale bar: 1 μm.

3.2 *Geobacter*'s viability in the imaging chamber

To ensure *Geobacter* cells were kept alive during the imaging process, we conducted an experiment in which we observed wild-type *Geobacter* under white light (Thorlabs SLS301, Figure 3.5) for 11 hours. We imaged a total of six filed of views for this experiment, in which we took 100 frames with a 100 ms camera exposure time every hour. We maintained almost the same experiment conditions as described in Chapter 2.4 for the imaging procedure for *Geobacter*, except that we put 1.5mL of anaerobic growth media as imaging buffer to provide nutrients for *Geobacter*

growth. Additionally, we constantly bubbled nitrogen instead of argon into the imaging chamber. All images (Figure 3.5) are the average from 100 frames processed by ImageJ, as they show the same field of view for different time points. Notably, there were no *Geobacter* cells inside the red square at 0h, whereas at least five *Geobacter* cells reside within it at 11h. These results indicate that even at a lower temperature (22°C) on our microscope than its optimal growth temperature (30°C), *Geobacter* cells were still viable and could grow inside our custom-made anaerobic imaging chamber.

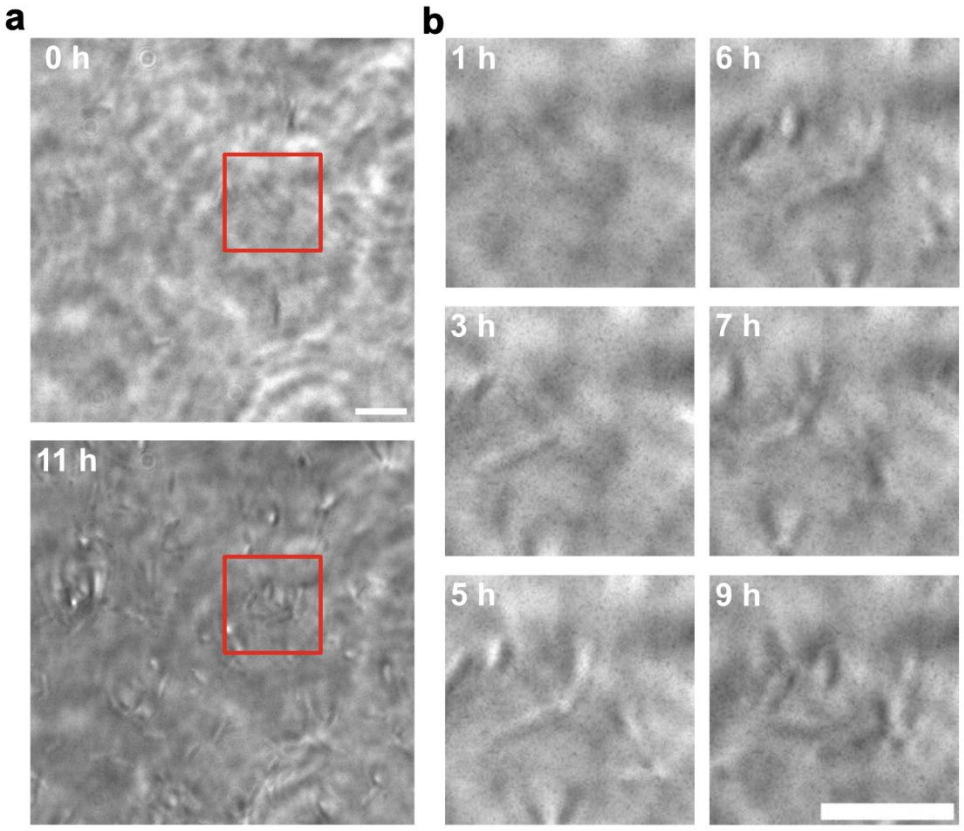

Figure 3. 5 *Geobacter* viability inside anaerobic chamber. Images in (a) show the bright field of wild type *Geobacter* on hour 0 and hour 11. Images (b) are enlarged images from the region within the red box in (a). Scale bar: 5 µm.

3.2 Single-molecule localization microscopy of *Geobacter*

3.3.1 Nile Red activity

In Section 3.1, we demonstrated the transient binding of Nile red to resolve the spherical morphology of SLB-coated glass spheres. Every SLB-coated glass bead seen in the bright field (BF) image was also detected via Nile red emission in the epifluorescence (FL) channel. However, the same was not observed for *Geobacter* Nile red imaging. Although we imaged over 200 *Geobacter* cells for both wild-type (Figure 3.6 and 3.7) and Δ5 *Geobacter* (Figure 3.6, 3.7, 3.8 and 3.9), only less than 10% (as indicated in Table 3.1) of them could be detected in the epifluorescence channel. Our hypothesis is that Nile red is reduced by a redox partner in or near the outer membrane, thereby shutting off its fluorescence.

Table 3. 1 *Geobacter* cell count in the bright field (BF) and epifluorescence (FL) imaging channels across different FOVs

	FOVs	Cell count in BF	Cell count in FL	Ratio of cells in FL vs. BF
Wild-type	6	290	22	7.59%
Δ5 mutant	13	253	23	9.10%

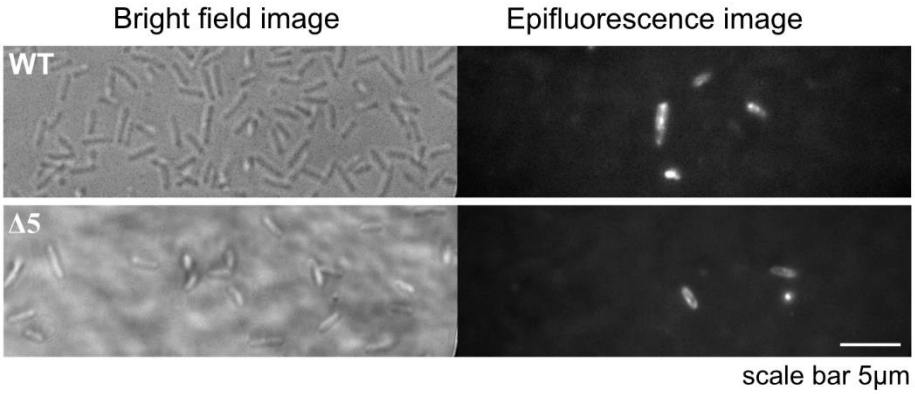

Figure 3. 6 Wild-type and Δ5 *Geobacter* Nile red activity. Scale bar: 5μm.

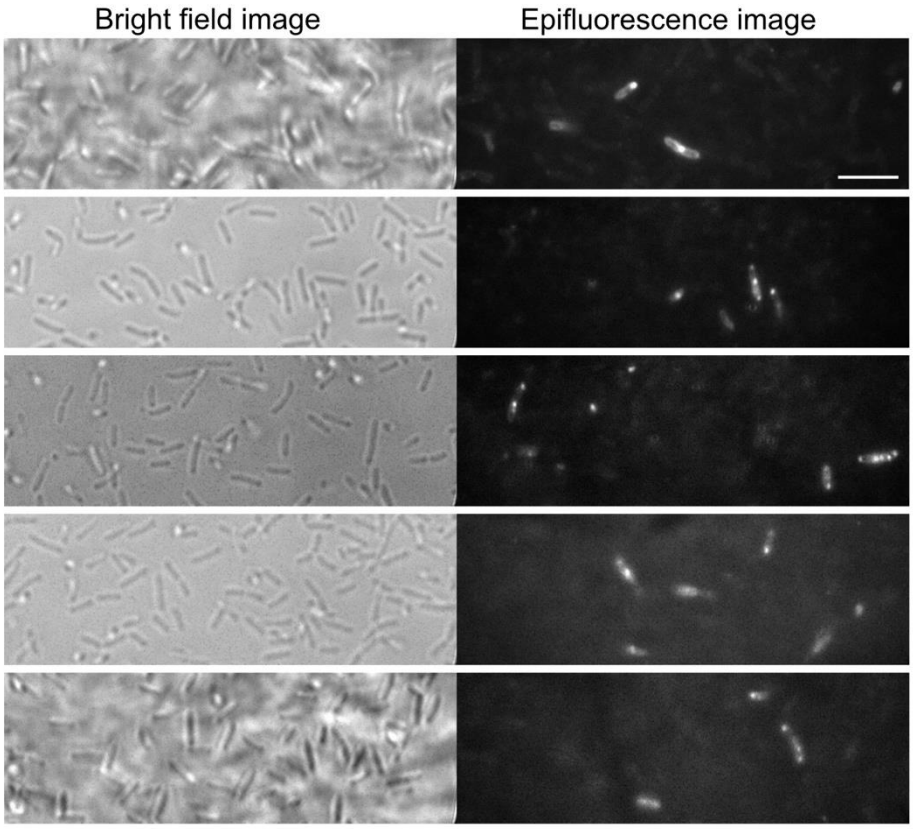

Figure 3. 7 Wild-type *Geobacter* Nile red activity. Scale bar: 5µm.

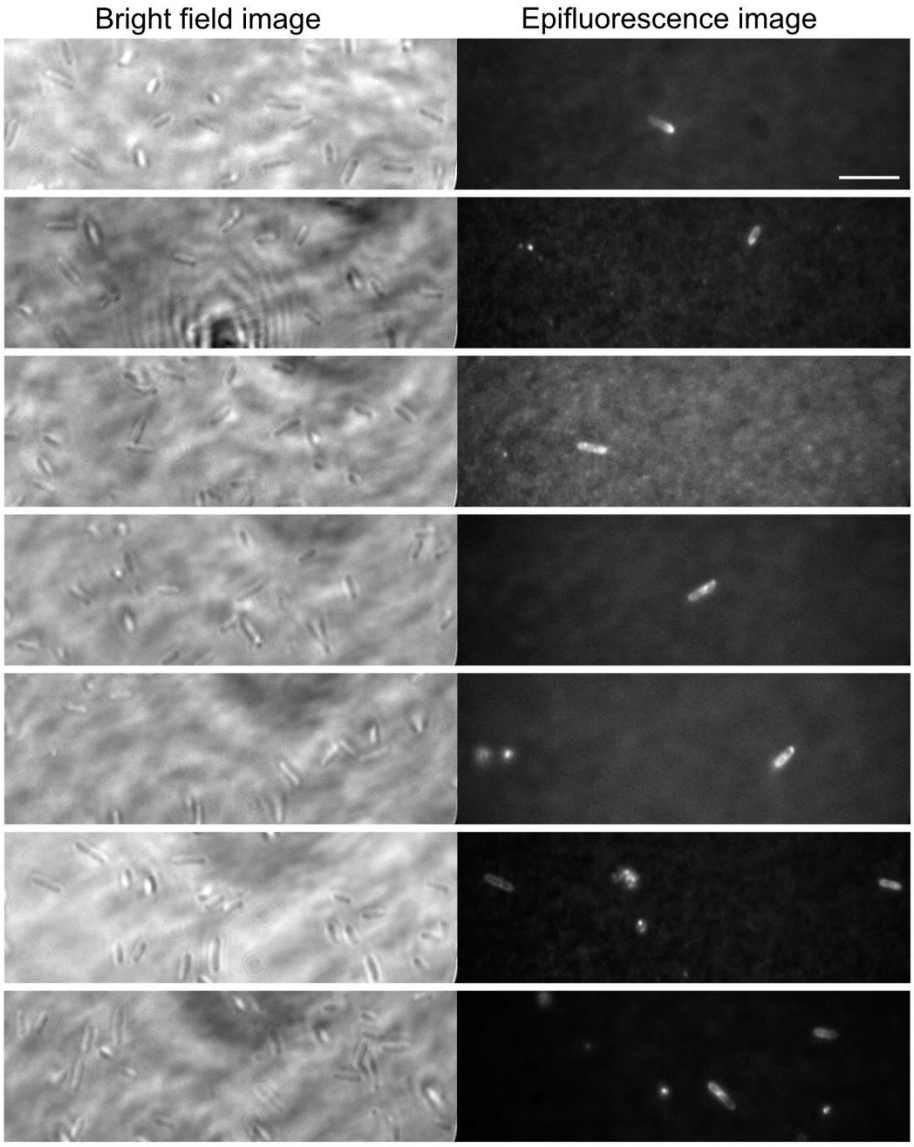

Figure 3. 8 Δ5 *Geobacter* Nile red activity. Scale bar: 5μm.

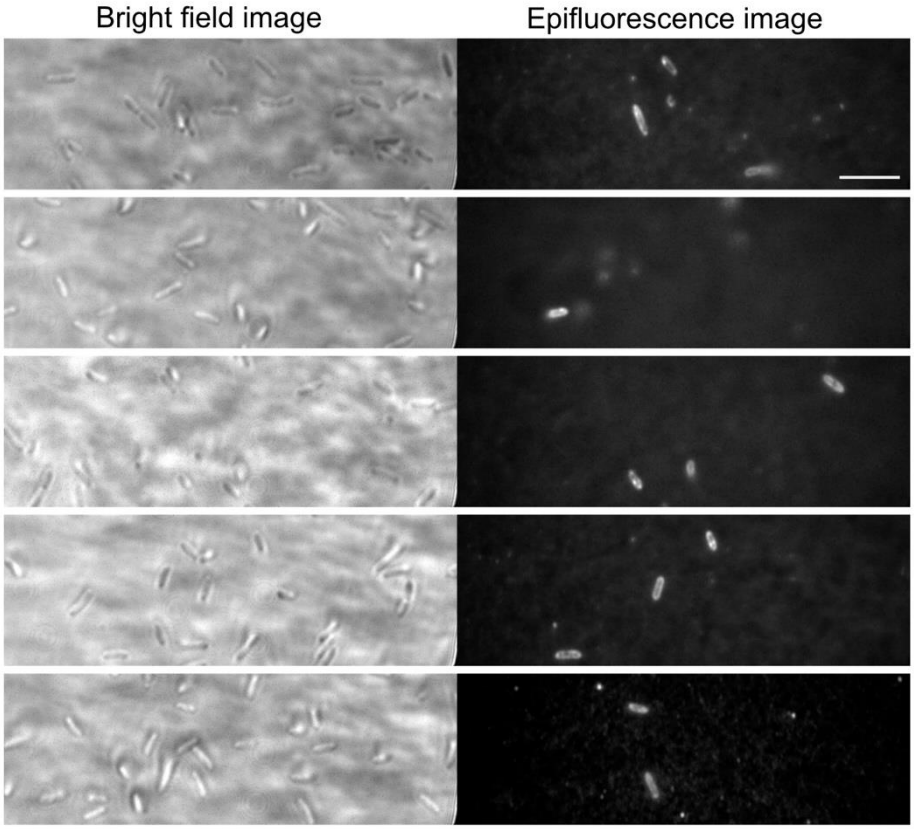

Figure 3. 9 Δ5 *Geobacter* Nile red activity. Scale bar: 5μm.

3.3.2 *Geobacter* Nile red spatial distribution

Utilizing Single-Molecule Localization Microscopy (SMLM), we were able to successfully reconstruct the rod-like shape of the *Geobacter*. However, we observed that the distribution of Nile red localizations is non-uniform, both between different cells on a single coverslip and along individual cell membranes. Interestingly, using same imaging conditions and SMLM image post-processing protocol, we found that the number of localizations per 20,000 frames for the wild-type *Geobacter* was only approximately one-fourth that of the Δ5 mutant. Additionally, we discovered that Nile red is much more active inside Δ5 cells, as shown in Figure 3.10 (a).

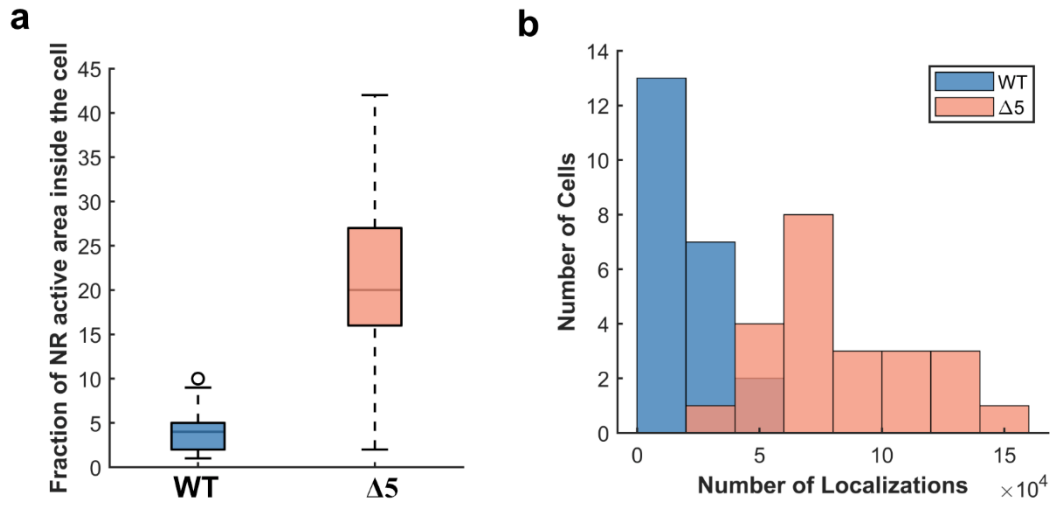

Figure 3. 10 Nile red activity and number of localizations quantifications. (a) Nile red activity inside the *Geobacter*. WT: wild-type *Geobacter*, 22 FOVs. Δ5: Δ5 *Geobacter*, 23 FOVs. (b) Number of localizations within each FOV.

Moreover, based on the Nile red distribution of the reconstructed SMLM images, we observed that Nile red localization patterns also significantly vary cell to cell. To further understand these patterns, we classified them into six different categories. Our analysis revealed that five classes appeared in the wild-type *Geobacter* (Figure 3.11 and 3.13), and three in the Δ5 *Geobacter* (Figure 3.12 and 3.14). The diffuse and the sparse activation species were only observed in the wild-type *Geobacter*, while over 50% of the cells were in the extended membrane group for the Δ5 *Geobacter*.

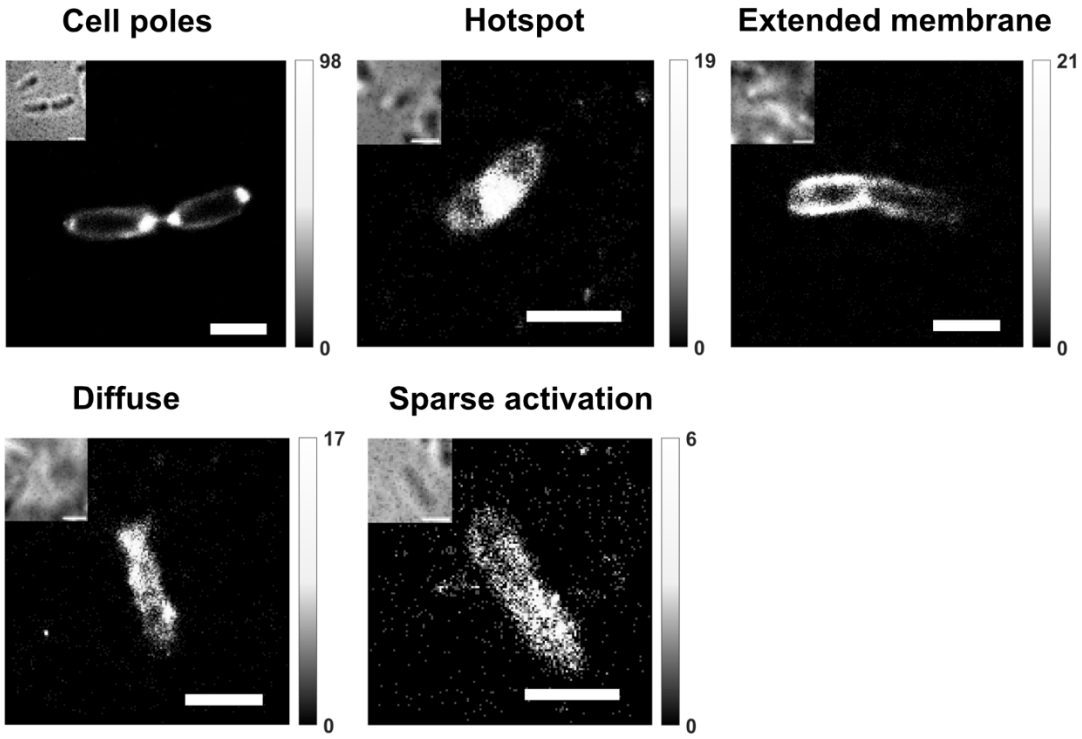

Figure 3. 11 Wild-type *Geobacter* Nile red spatial distribution classes. Cell poles: Only one or both poles have clustered localizations. Hotspot: One or more localized clusters. Extended membrane: Localizations are concentrated along membrane. Color bar: Number of localizations per bin (bin size: 20 nm × 20 nm). Scale bar: 1 μm.

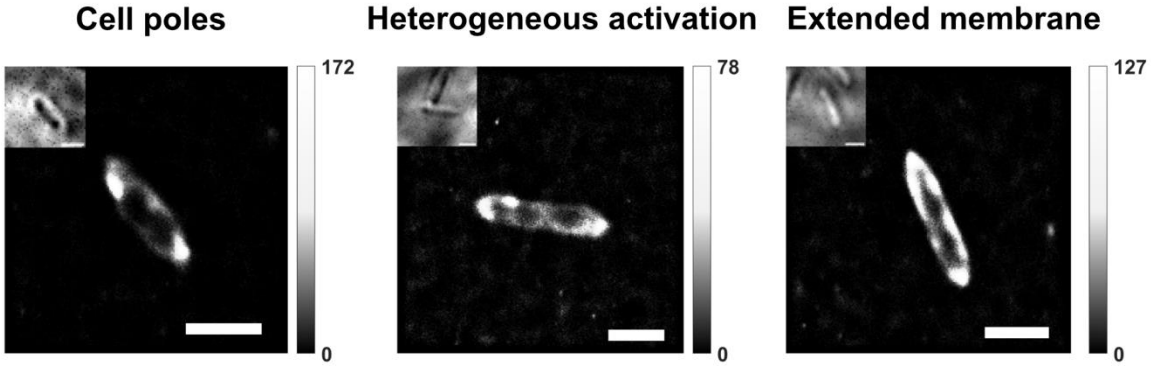

Figure 3. 12 Δ5 *Geobacter* Nile red spatial distribution classes. Cell poles: Only one or both poles have clustered localizations. Heterogeneous activation: Complex localization pattern. Extended membrane: Localizations are concentrated along membrane. Color bar: Number of localizations per bin (bin size: 20 nm × 20 nm). Scale bar: 1 μm.

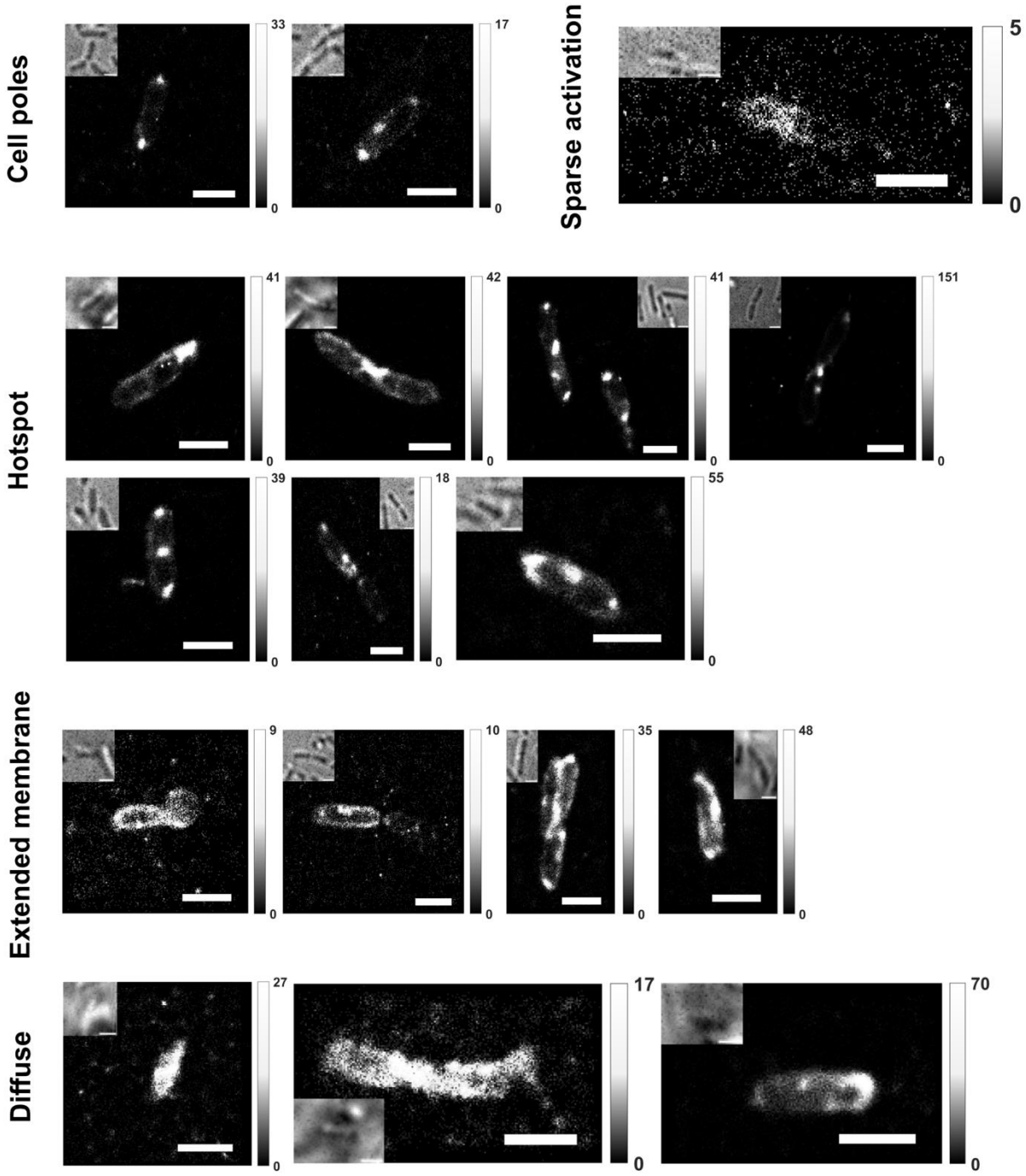

Figure 3. 13 Wild-type *Geobacter* Nile red spatial distribution classes. Color bar: Number of localizations per bin (bin size: 20 nm × 20 nm). Scale bar: 1 μm.

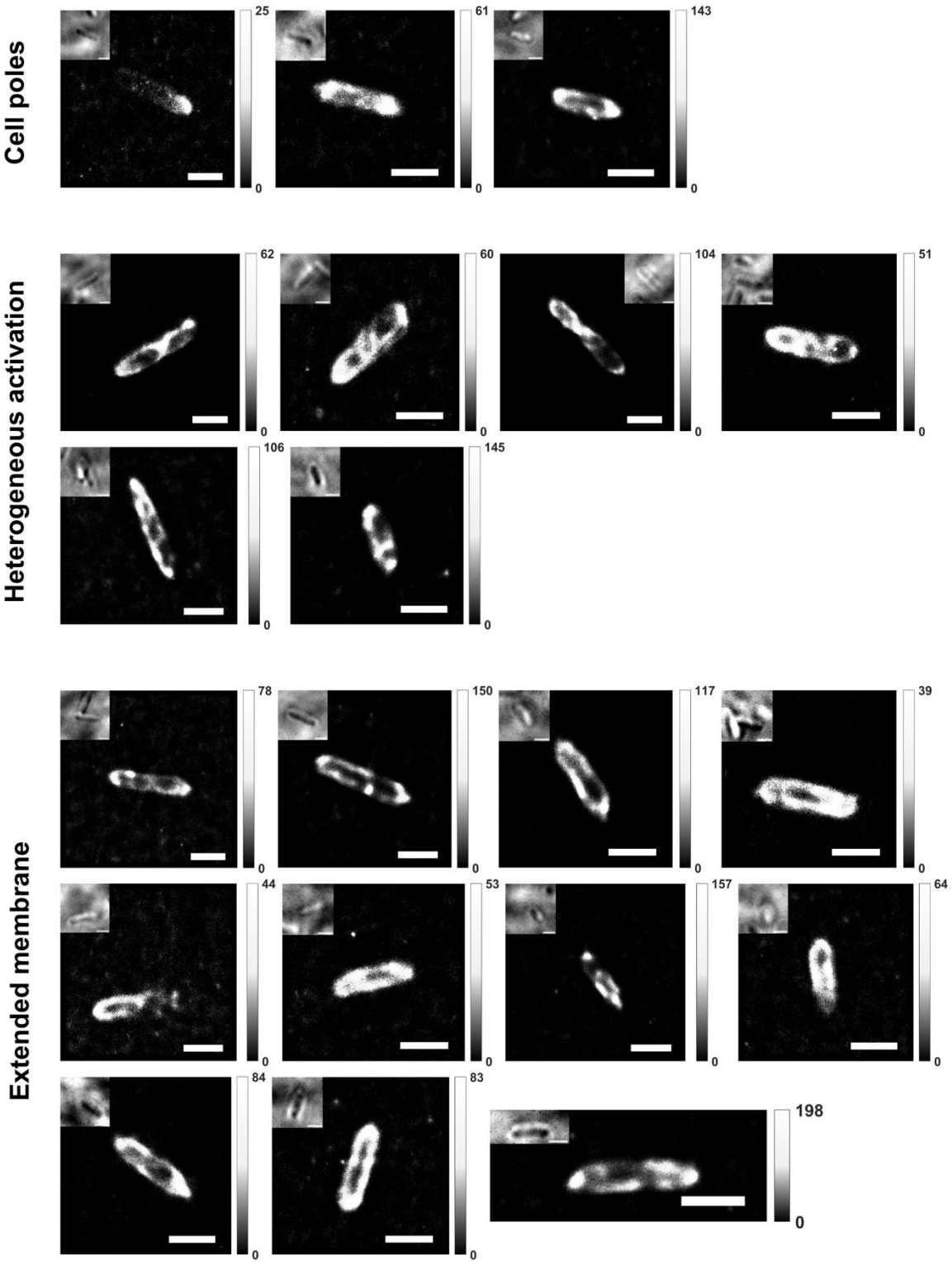

Figure 3. 14 Δ5 *Geobacter* Nile red spatial distribution classes. Color bar: Number of localizations per bin (bin size: 20 nm × 20 nm). Scale bar: 1 μm.

3.3.3 Fluorescence burst durations of Nile red

We also quantified the burst duration of Nile red molecules using consecutive frames (as described in Chapter 2) for *Geobacter*. We compared SMLM images plotted using molecules whose burst durations were longer than and shorter than 60 ms (Figure 3.15 and 3.16). Interestingly, we found that for the cell poles, hotspot, extended membrane and the heterogeneous activation classes, the long-lived Nile red (burst duration larger than 20 ms) molecules were not uniformly distributed throughout the cell.

As shown in Figure 3.4, the burst durations of Nile red molecules were slightly longer with no oxygen present. After plotting the percentage of burst durations over 60 ms for wild-type and Δ5 *Geobacter*, we discovered that the median percentage for and Δ5 *Geobacter* was twice as high as wild-type *Geobacter* (Figure 3.17), indicating that the Δ5 species tend to have more molecules with longer burst durations. We also found that the mean burst duration of the Δ5 *Geobacter* was 20 ms longer than those within wild-type.

We hypothesize that the heterogeneous Nile red fluorescence burst durations result from the various redox and membrane environments within each cell, enabling NR to find locations to bind to and maintain fluorescence for a long time.

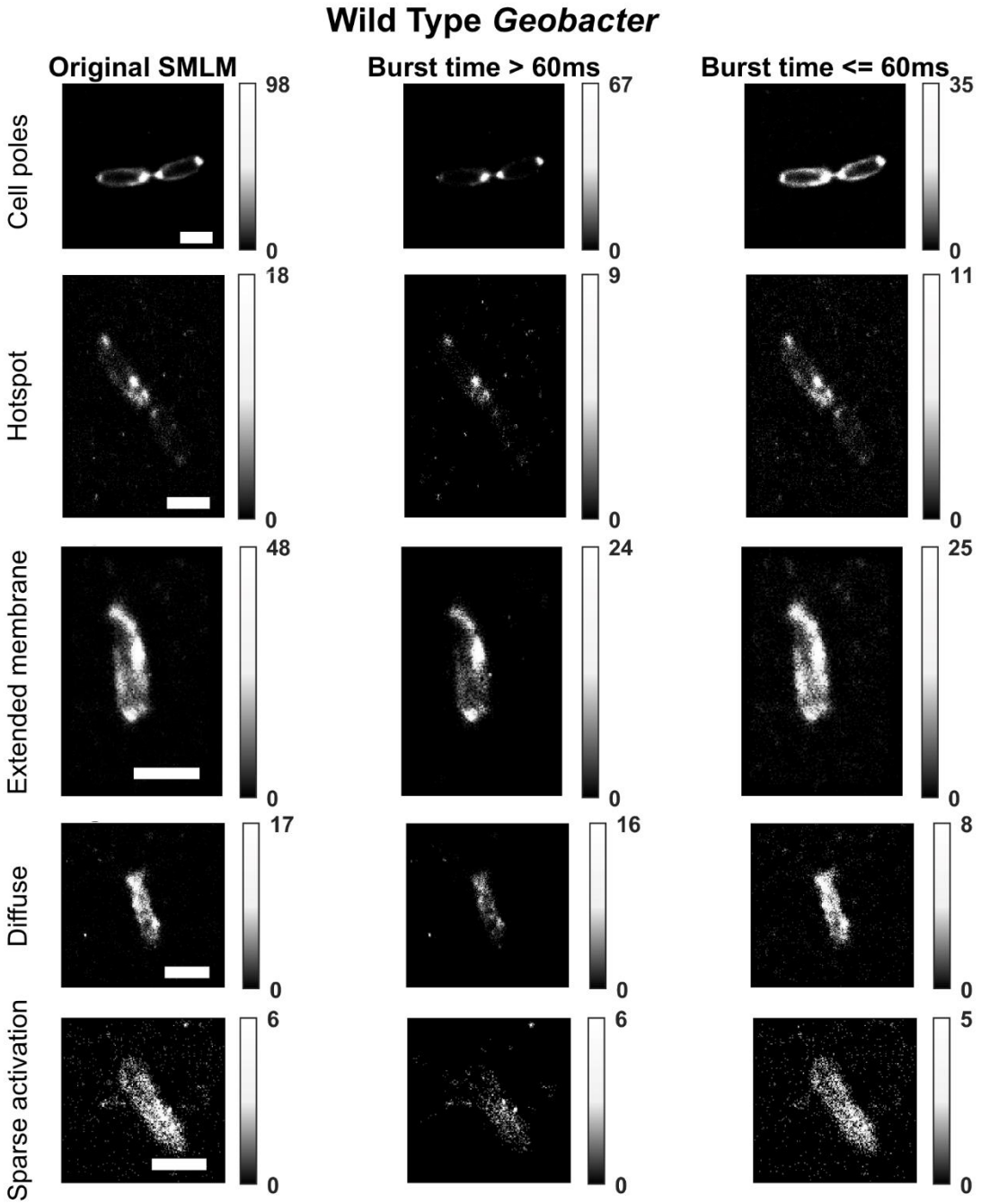

Figure 3. 15 SMLM images of wild-type *Geobacter* using molecules with burst durations over and under 60 ms. Different rows show one cell from five different classes for Wild-type *Geobacter*. Scale bar: 1 μm.

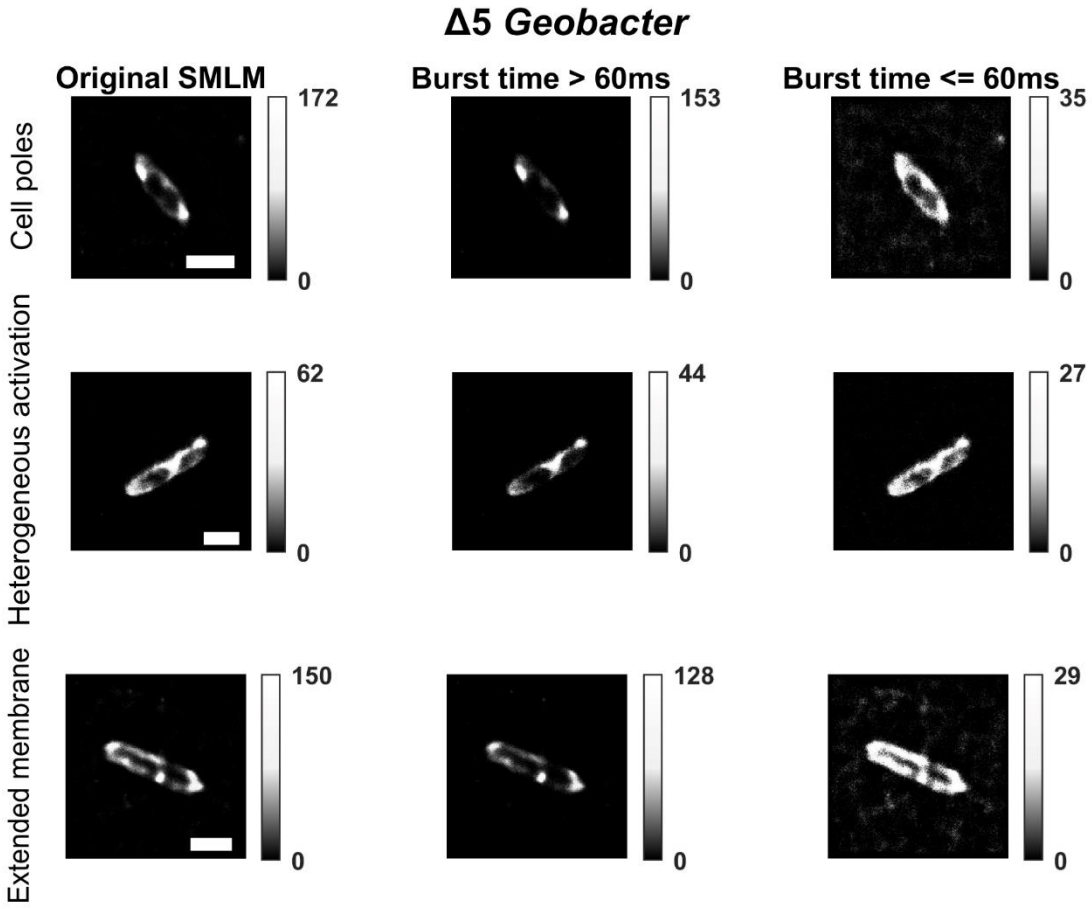

Figure 3. 16 SMLM images of Δ5 *Geobacter* using molecules with burst durations over and under 60 ms. Different rows show one cell from four different classes for Δ5 *Geobacter*. Scale bar: 1 μm.

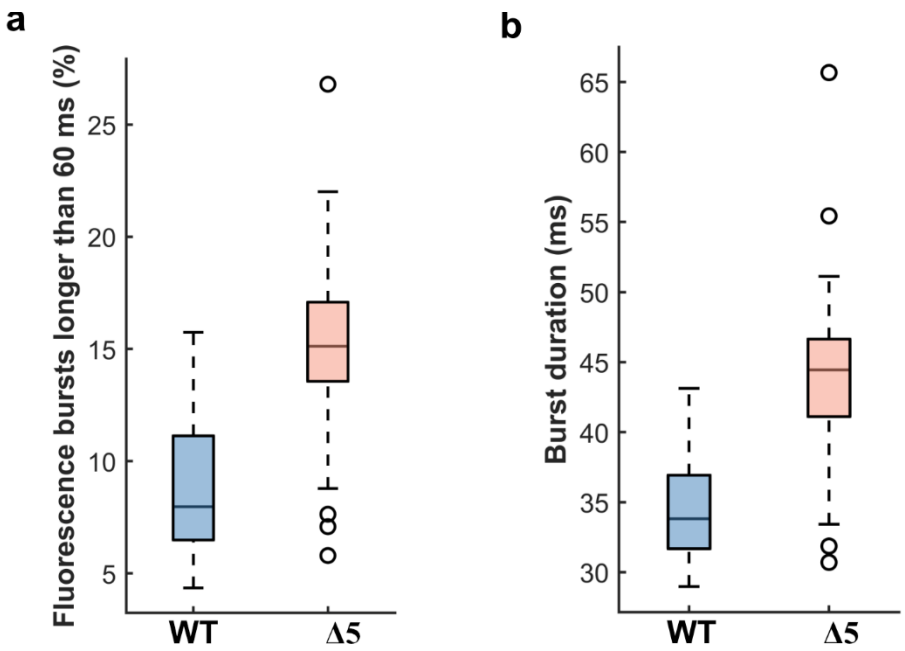

Figure 3. 17 *Geobacter* Nile red burst duration comparison. (a) Fraction of molecules whose fluorescence bursts lasted longer than 60ms. (b) Mean burst duration.

3.3.4 *Geobacter* cell dynamics

When analyzing the relationship between the number of localizations and the frame number, we observe a significant difference in Nile red binding behavior between three Δ5 *Geobacter* within the same large field of view. Specifically, the number of localizations from frame 10,000 to 15,000 (as shown in Figure 3.18) shows a clear drop for the first cell but not for the other two cells. These variations in Nile red blinking behavior provides direct evidence that the *Geobacter* was indeed alive during imaging process.

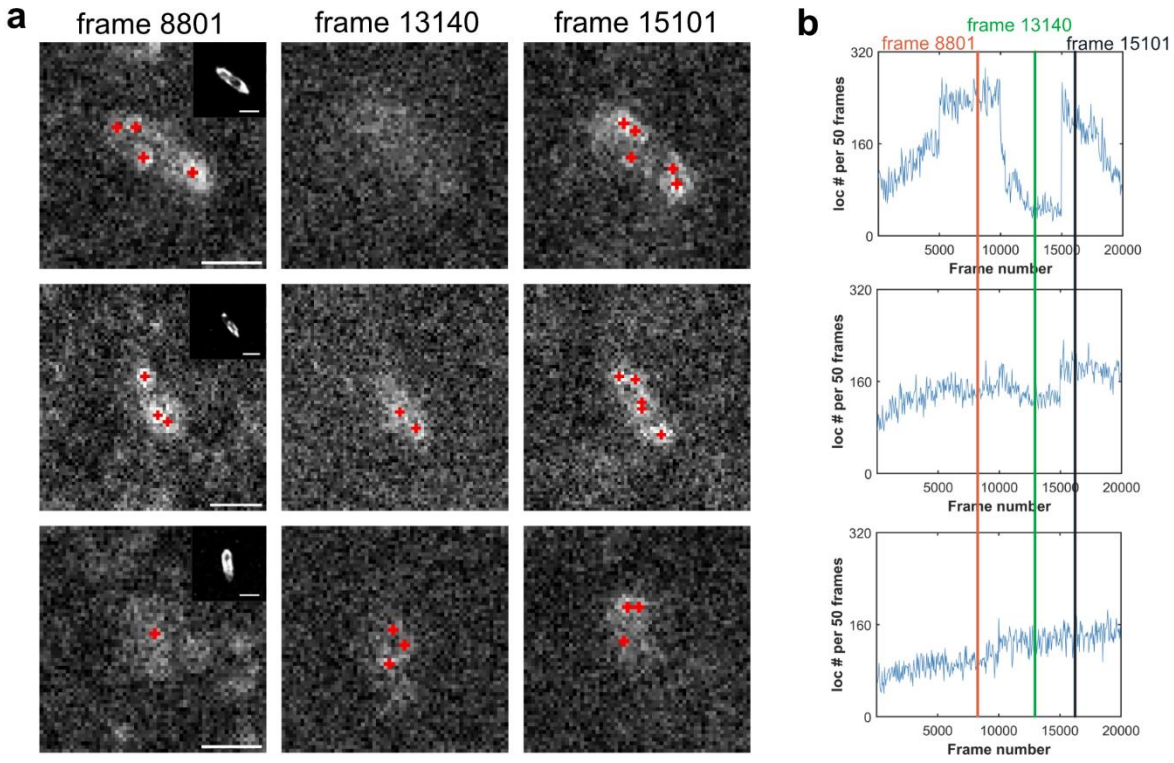

Figure 3. 18 *Geobacter* cell dynamics. (a) Raw images of three *Geobacter* within the same FOV with the red cross as the center of the point spread function. Inset: SMLM reconstructed image. (b) Number of localizations per 50 frames. Scale bar: 1 μm.

Chapter 4: Summary and outlook

In this thesis, we have successfully performed single-molecule imaging of lipid-coated glass spheres and *Geobacter* at nanoscale resolution under anaerobic conditions. Our findings have revealed that Nile red does not turn on in every *Geobacter* membrane, which may be attributed to the redox activity of each cell. We have also observed different localization behaviors of Nile red between the wild-type and the Δ5 mutant, as well as variations between cells, which could impact the intra-cell electrochemical conditions when cytochromes are deleted. Additionally, we have found heterogeneity in the fluorescence burst durations of Nile red which could be due to variations in redox and membrane environments within each cell, allowing Nile red to bind and maintain fluorescence for a long time.

In further studies, we could use the external electrode to modulate the applied potential and observe how it affects the Nile red distribution in the *Geobacter* cell. Additionally, we could alter the imaging media by adding redox shuttles along with the Nile red dye to observe any changes in our observations.

References

[1] F. Caccavo, D. J. Lonergan, D. R. Lovley, M. Davis, J. F. Stolz, and M. J. Mcinerneyl, *Geobacter Sulfurreducens Sp. Nov., a Hydrogen-and Acetate-Oxidizing Dissimilatory Metal-Reducing Microorganism*, Appl. Environ. Microbiol. **60**, 3752 (1994).

[2] F. J. Otero, C. H. Chan, and D. R. Bond, *Identification of Different Putative Outer Membrane Electron Conduits Necessary for Fe(III) Citrate, Fe(III) Oxide, Mn(IV) Oxide, or Electrode Reduction by Geobacter Sulfurreducens*, J. Bacteriol. **200**, e00347 (2018).

[3] M. J. Rust, M. Bates, and X. Zhuang, *Sub-Diffraction-Limit Imaging by Stochastic Optical Reconstruction Microscopy (STORM)*, Nat. Methods **3**, 793 (2006).

[4] E. Betzig, G. H. Patterson, R. Sougrat, O. W. Lindwasser, S. Olenych, J. S. Bonifacino, M. W. Davidson, J. Lippincott-Schwartz, and H. F. Hess, *Imaging Intracellular Fluorescent Proteins at Nanometer Resolution*, Science (80-.). **313**, 1642 (2006).

[5] W. E. Moerner and D. P. Fromm, *Methods of Single-Molecule Fluorescence Spectroscopy and Microscopy*, Rev. Sci. Instrum. **74**, 3597 (2003).

[6] G. Donnert, J. Keller, R. Medda, M. Alexandra Andrei, S. O. Rizzoli, R. Lü hrmann, R. Jahn, C. Eggeling, and S. W. Hell, *Macromolecular-Scale Resolution in Biological Fluorescence Microscopy*, Proc. Natl. Acad. Sci. **103**, 11440 (2006).

[7] A. Sharonov and R. M. Hochstrasser, *Wide-Field Subdiffraction Imaging by Accumulated Binding of Diffusing Probes*, Proc. Natl. Acad. Sci. **103**, 18911 (2006).

[8] M. D. Lew, S. F. Lee, J. L. Ptacin, M. K. Lee, R. J. Twieg, L. Shapiro, and W. E. Moerner, *Three-Dimensional Superresolution Colocalization of Intracellular Protein Superstructures and the Cell Surface in Live Caulobacter Crescentus*, Proc. Natl. Acad. Sci. **108**, E1103 (2011).

[9] S. Choi, *Lack of Speci Fi City in Geobacter Periplasmic Electron Transfer*, J. Bacteriol. **204**, e00322 (2022).

[10] M. Ovesný, P. Křížek, J. Borkovec, Z. Švindrych, and G. M. Hagen, *ThunderSTORM: A Comprehensive ImageJ Plug-in for PALM and STORM Data Analysis and Super-Resolution Imaging*, Bioinformatics **30**, 2389 (2014).

[11] C. A. Schneider, W. S. Rasband, and K. W. Eliceiri, *NIH Image to ImageJ: 25 Years of Image Analysis*, Nat. Methods **9**, 671 (2012).

[12] C. E. Aitken, R. A. Marshall, and J. D. Puglisi, *An Oxygen Scavenging System for Improvement of Dye Stability in Single-Molecule Fluorescence Experiments*, Biophys. J. **94**, 1826 (2008).

[13] S. R. Jung, Y. Deng, C. Kushmerick, C. L. Asbury, B. Hille, and D. S. Koh, *Minimizing ATP Depletion by Oxygen Scavengers for Single-Molecule Fluorescence Imaging in Live*

Cells, Proc. Natl. Acad. Sci. U. S. A. **115**, E5706 (2018).

[14] T. Ding, K. Spehar, J. Bieschke, and M. D. Lew, *Long-Term, Super-Resolution Imaging of Amyloid Structures Using Transient Amyloid Binding Microscopy*, in *Proceedings of SPIE* (SPIE-Intl Soc Optical Eng, 2019), p. 19.